Autocorrelation-Based Spectrum Sensing of FBMC Signal

Upender Keesara, Sachin Chaudhari
Signal Processing and Communication Research Center
Center of Excellence in Signal Processing
International Institute of Information Technology
Hyderabad-500032, INDIA
Email: keesara.upender@research.iiit.ac.in, sachin.chaudhari@iiit.ac.in

***Abstract*—The focus of this paper is on a feature detector for filter bank multicarrier (FBMC) signal in cognitive radio. In this paper, we first prove that the FBMC signal samples are uncorrelated with each other. However, if the FBMC signal is processed by our proposed method, then the autocorrelation function (ACF) of FBMC signal becomes non-zero at the lag equal to number of subcarriers. On the other hand, additive white Gaussian noise (AWGN) samples after the same proposed processing remain uncorrelated. Using this feature, an autocorrelation based feature detector is proposed to detect FBMC signal in noise. The main advantage of the proposed detector is that, unlike blind detectors, this detector can distinguish between FBMC signal and noise (or interference). Next, the distribution of the test statistic of the proposed detector is derived under noise-only scenario so that the threshold of the Neyman-Pearson detector can be designed to maintain constant false alarm rate while maximizing the probability of detection. Simulation results demonstrate the efficacy of the proposed detector.**

***Index Terms*—Autocorrelation, cognitive radio, FBMC signal, feature detector.**

I. Introduction

Orthogonal Frequency Division Multiplexing (OFDM) has been a dominant technology in 4G LTE-Advanced. However, OFDM might be a misfit for future generation cellular technologies such as 5G and cognitive radios due to some disadvantages such as loss in spectral efficiency due to cyclic prefix (CP) insertion, high out-of-band radiation and sensitivity to narrowband interferers [1]–[3]. As shown in main outcomes of EU research projects 5GNOW [1] and PHYDYAS [4], filter bank multicarrier (FBMC) is a promising alternative to OFDM for 5G and cognitive radios, respectively. FBMC uses well designed bank of filters with minimum out-of-band radiation and no use of CP means significant improvement in the spectral efficiency [5].

Spectrum sensing is one of the most important tasks in cognitive radios. In the traditional cognitive radio standards, the main problem has been to detect the presence of primary (licensed or legacy) user using incumbent geolocation databases and spectrum sensing techniques [6]. However, the challenging problem of heterogeneous secondary coexistence has garnered very less attention in the cognitive radio standards and related literature [7]. Since 5G will involve multitier heterogeneous networks in heterogeneous bands (licensed as well as unlicensed), acquiring spectrum awareness regarding the secondary users is equally important. Moreover, the use of new waveforms in 5G PHY will necessitate design of the spectrum sensing algorithms for the new candidate waveforms. As FBMC is one of the few most potential candidates for 5G waveform [2], [8], sensing and distinguishing FBMC signal is a very relevant problem. As such, the focus of this paper is on proposing spectrum sensing scheme for FBMC signal.

In spectrum sensing literature, most of the detection schemes have been designed for OFDM signal [6] and there is a dearth of research on spectrum sensing of FBMC signal. Although blind detection techniques such as energy detection can be used to detect any waveform, they cannot distinguish between noise and interfering signal. In addition they have serious issues such as SNR walls [9]. In [10], a feature detector was proposed based on the induced repeating patterns in the transmitted FBMC signal. Thus there is a dearth of feature detectors for FBMC signal in the spectrum sensing literature. With this as motivation, a feature detector is proposed in this paper which can distinguish between FBMC-plus-noise and noise-only scenarios. Also unlike [10], no attempt is being made to induce patterns in the basic FBMC transmission.

The specific contributions of this paper are:

- It is shown that the autocorrelation function (ACF) of the FBMC signal is zero for non-zero lags.
- After proper study of FBMC signal generation, a method is proposed to process the FBMC signal at the receiver so that the processed FBMC signal has non-zero ACF value at a certain lag value other than zero. On the other hand, if the same processing is applied to AWGN samples, the processed noise samples remain uncorrelated.
- A spectrum sensing scheme is proposed to detect the differences in ACF behavior of the processed (or modified) data in the two scenarios of FBMC-plus-noise and noise-only.
- The conditional distribution of the proposed test statistic, conditioned on the received signal being only noise, is derived so that the threshold for Neyman-Pearson detector can be evaluated analytically.

This paper is organized as follows. Section II describes the FBMC signal generation while Section III presents the autocorrelation analysis of the received FBMC signal as well

978-1-5386-1182-1/18/$31.00 ©2018 IEEE

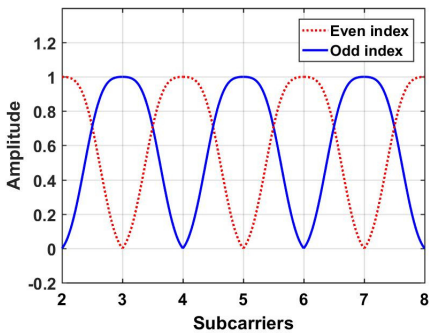

Fig. 1: A portion of the filter-bank for overlapping factor, $K = 3$. Here, odd-index and even-index subchannels are separated and there is overlap between adjacent subchannels only [5].

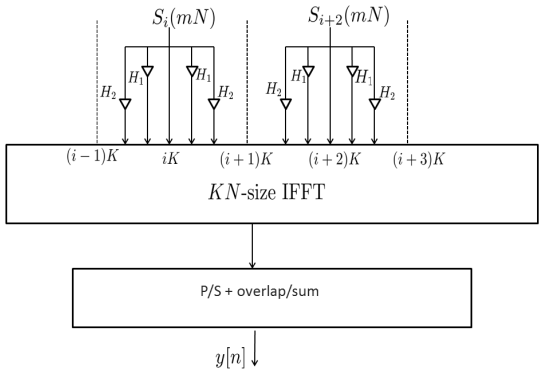

Fig. 2: Weighted frequency spreading and extended IFFT for $K = 3$. Here, i is subcarrier index, m is symbol index and N is number of subcarriers [5].

its proposed modified version. In Section IV, distribution of the proposed test statistic is derived and detection of FBMC signal is explained using the proposed detection scheme. In Section V, results are presented. Finally, section VI concludes this paper.

II. FBMC Signal Structure

FBMC is a multicarrier transmission technique that is an attractive alternative to the OFDM technique. In OFDM, FFT acts like a filter using rectangular window in time domain which amounts to frequency response at each subcarrier (or subchannel) being a sinc function. The sinc function has high side-lobes resulting in out-of-band ripples. In FBMC, in order to reduce the out-of-band ripples, the main-lobe of filter-frequency-response at each subcarrier is spreaded while side-lobes are reduced so that only adjacent subchannels are overlaping as shown in Fig. 1. In the figure, the even (or odd) indexed subchannels are separated and there is overlap between adjacent subcarriers. As a result of spreading the main-lobe in frequency, the subcarriers are no longer orthogonal in FBMC as they were in OFDM. However, there are several advantages of this design: side-lobes are significantly lesser as compared to OFDM, no inter-channel-interference from all subcarriers (except from the immediate neighbors) as in OFDM in the presence of carrier frequency offset. The orthogonality between adjacent subchannels in FBMC can be achieved using offset quadrature amplitude modulation (OQAM) modulation technique. In this paper, we consider OQAM-FBMC implementation employed in [5], [11].

As overall frequency spread of the response has significantly reduced in FBMC, the impulse response of the filter spreads in time beyond one symbol period and the symbols overlap in time domain. The number of symbols that overlap in time domain is given by the parameter K, known as *overlapping factor*. In this paper, the overlapping factor considered is $K = 3$. The design of the *prototype filter* (or the first filter in the filter-bank) is based on Nyquist criterion as explained in [5]. Next, the filter bank is obtained by multiplying the prototype filter coefficients by $e^{\frac{j2\pi ln}{N}}$ where l is the index of l^{th} filter in the bank and n is the index of input data element given to IFFT.

In OFDM, each data element given to the subcarrier of the $N-$size IFFT block modulates a single carrier whereas in filter-bank, each data element applied to $KN-$size IFFT modulates $(2K-1)$ sub-carriers due to the overlapping factor K. Thus, single data element is spread over many IFFT inputs. This operation is known as *weighted frequency spreading* [5]. As shown in Fig. 2, input element $S_i[mN]$, with $0 \leq i \leq (N-1)$ and m as the symbol index, modulates $(2K-1)$ carriers centered at iK subcarrier. The Prototype filter frequency coefficients are chosen in such a way that they satisfy Nyquist criterion for zero ISI [12]. These filter coefficients are obtained as [13]:

$$\begin{aligned} &H_0 = 1 \quad ; \quad H_k^2 + H_{K-k}^2 = 1 \quad ; \\ &H_{KN-k} = H_k \quad ; \quad 1 \leq k \leq K-1 \\ &H_k = 0 \quad ; \quad K \leq k \leq KN-K, \end{aligned} \tag{1}$$

where N is number of subcarriers. Hence, using (1), the weights for $K = 3$ are obtained as $H_0 = 1$, $H_1 = H_{-1} = 0.911438$ and $H_2 = H_{-2} = 0.411438$. The corresponding impulse response $\mathbf{h}$ of length $KN = 192$ samples is shown

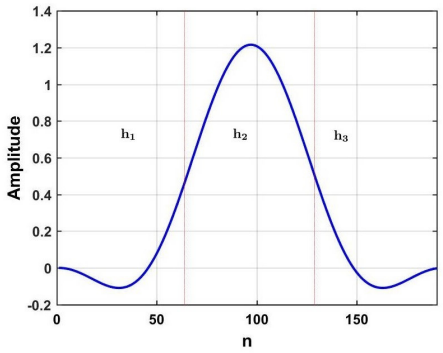

Fig. 3: Impulse response of prototype filter for $K = 3$ and $N = 64$ subcarriers. Here, n is discrete time index.

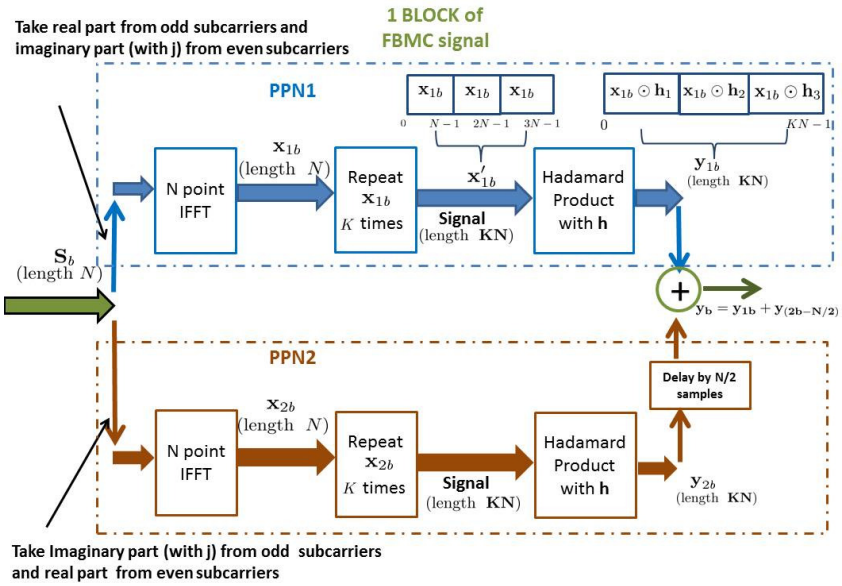

Fig. 4: FBMC block diagram: This figure shows the generation of b^{th} block of data samples. Each input block ($\mathbf{S_b}$) is of length N samples and output block ($\mathbf{y_{1b}}$ or $\mathbf{y_{2b}}$) is of length KN samples. Output samples of PPN2 are delayed by $\frac{N}{2}$ samples and are added to ouput samples of PPN1 to give corresponding b^{th} block output.

in Fig. 3 for $K = 3$ and $N = 64$ subcarriers. The figure also shows the three equal partitions of $\mathbf{h}$, i.e., $\mathbf{h}_1$, $\mathbf{h}_2$, $\mathbf{h}_3$ which will play important role in simplifying the analysis in later sections.

In OQAM technique, the real and imaginary parts of a complex symbol are delayed by half the symbol time and are not transmitted simultaneously, thus making the subcarriers orthogonal. The delay of half the symbol time introduced here reduces the capacity of the system. Hence, to achieve full capacity the symbol rate is doubled and two poly-phase networks (PPNs) are employed for low-complexity implementation of OQAM-FBMC so that the size of IFFT block reduces from KN to N [5]. As the focus of this paper is not to explain the efficient OQAM-FBMC implementation using PPNs, we direct interested readers to [5], [11] for discussion on actual efficient implementations of OQAM-FBMC using PPNs.

Next, we explain the FBMC signal generation described and implemented in [11], which is helpful in finding the structure in the FBMC signal, which in turn can be detected using a feature detector. Note that the implementation of weighted frequency spreading shown in Fig. 2 can be achieved by first loading every K^{th} subcarrier with data and then convolving with frequency response $H(k)$ of prototype filter, where k is subcarrier index. In time domain, this is equivalent to repeating the time-domain data-block K times and then multiplying the resultant data vector of length KN with $\mathbf{h}$. This approach is used in this paper to generate the FBMC signal and is shown in Fig. 4. The FBMC transmitter section is shown in Fig. 4. Complex QAM/PSK symbols, $S[i]$, are fed to N-IFFT block of both PPN1 and PPN2 sections. In PPN1, real part of data is loaded on to sub-carriers of odd indices and imaginary part of data is loaded on to sub carriers of even indices. The PPN1 data vector corresponding to b^{th} block is represented by $\mathbf{x}_{1b}$. On the other hand, in PPN2, imaginary part of data is loaded on to odd subcarriers and real part of data is loaded on to even subcarriers. Each output block of KN samples of PPN1 and PPN2 overlap by $\frac{N}{2}$ samples and the samples are added to give the transmitted FBMC signal $y[n]$. Here, $y[n] = y_1[n] + y_2[n - N/2]$ where $y_1[n]$ and $y_2[n]$ are the outputs of PPN1 and PPN2 sections, respectively.

Fig. 5 shows a representative example of the frame structure of FBMC signal assuming $K = 3$ and 7 input data blocks $\mathbf{S}_b$ of N samples with $b = 1, 2, \ldots, 7$. Generation of PPN1 is shown in Fig. 5. Each block is delayed by N samples to its preceding block and these blocks are overlapped to give a final frame. Generation of PPN2 will be similar and only the resulting PPN2 frame is shown. Note that the autocorrelation operation has to be done on a *steady state frame*, which is defined as the part of the transmitted frame containing K number of overlapped symbols for both PPN1 and PPN2. A steady state frame is obtained by removing KN samples, from the overlapped frames, at the beginning and $(K-1)N$ samples at the end. This steady state frame is only considered for autocorrelation analysis.

III. Autocorrelation Analysis of FBMC Signal

Note that the feature detector proposed in this paper is going to be implemented at the receiver. As this section focuses only on analyzing the ACF for FBMC signal, we assume noise-free channel in this section so that the received as well as transmitted FBMC signals are same. We first start with ACF analysis of the received FBMC signal to show that the

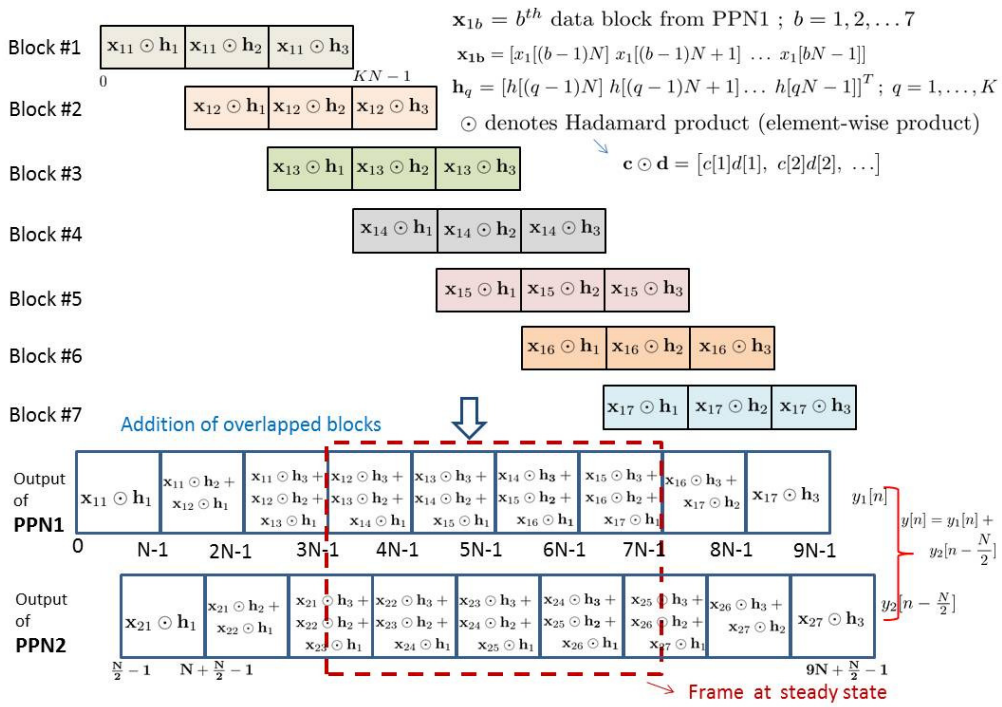

Fig. 5: Representation of FBMC frame structure. In this figure, generation of PPN1 is shown using blocks. Generation of PPN2 will be similar and only the resulting PPN2 frame is shown. Here, $K = 3$, number of blocks = 7.

autocorrelation values at non-zero lags ($\tau \neq 0$) are zero. Next, based on the study of FBMC signal generation, we propose the modification to the FBMC signal at the receiver such that autocorrelation values at $\tau = N$ become non-zero. This is followed by ACF analysis of modified FBMC signal at the receiver and derivation of closed form expression for the corresponding non-zero autocorrelation values at $\tau = N$.

A. ACF analysis of the received FBMC signal without any modifications

Output of PPN1 is $y_1[n] = x_1[n]h[n]$ and output of PPN2 is $y_2[n] = x_2[n]h[n]$. Here, $x_1[n]$ and $x_2[n]$ are IFFT output symbols of PPN1 and PPN2 sections respectively. Now using $y[n] = y_1[n] + y_2[n - \frac{N}{2}]$ and orthogonality of $y_1[n]$ and $y_2[n]$ (since they are output of different PPNs of OQAM-FBMC

$$R_y(n,\tau) = E\{y[n]y^*[n+\tau]\} = \sum_{k=0}^{K-1} \Big(E\big\{x_1[n+kN]h[n+kN]x_1^*[n+kN+\tau]h^*[n+kN+\tau]\big\} + E\big\{x_2[n+kN-\frac{N}{2}]h[n+kN-\frac{N}{2}]x_2^*[n+kN-\frac{N}{2}+\tau]h^*[n+kN-\frac{N}{2}+\tau]\big\}\Big)$$

$$= \begin{cases} \sigma_x^2 \sum_{k=0}^{K-1} \Big(h[n+kN]h^*[n+kN+\tau] + h[n+kN-\frac{N}{2}]h^*[n+kN-\frac{N}{2}+\tau] \Big) & \tau = 0, N, 2N \\ 0 & \tau \neq 0, N, 2N \end{cases} \tag{2}$$

Owing to $\mathbf{h}$ being a Nyquist pulse,

$$\sum_{k=0}^{K-1} \Big(h[n+kN]h^*[n+kN+\tau] + h[n+kN-\frac{N}{2}]h^*[n+kN-\frac{N}{2}+\tau] \Big) = 0$$

for $\tau = N, 2N$ so that

$$\therefore R_y(n,\tau) = \begin{cases} \sigma_x^2 \sum_{k=0}^{K-1} \Big(h^2[n+kN] + h^2[n+kN-\frac{N}{2}] \Big) & \tau = 0 \\ 0 & \tau \neq 0 \end{cases} \tag{3}$$

implementation), the ACF of $y[n]$ for the steady state frame can be calculated theoretically from Fig. 5 as given by (3).

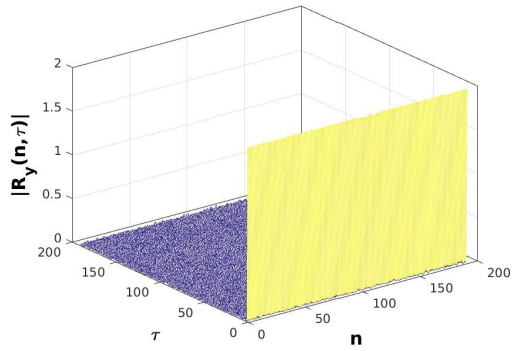

Fig. 6: Simulated autocorrelation of the received FBMC signal with out any modification. The number of Monte-Carlo realizations = 10000. The autocorrelation values are zero for non-zero lags.

Fig. 6 shows the autocorrelation of $y[n]$ for different τ values. The autocorrelation value is non-zero for $\tau = 0$ and the value is zero for $\tau \neq 0$. The signal $y[n]$ exhibits no correlation property except for zero-lag.

B. Proposed modification to the received FBMC signal and corresponding ACF

Let $\mathbf{y}' = [y[3N],\ y[3N{+}1],\ y[3N{+}2],\ \ldots,\ y[N_fN{+}3N{-}1]]$ be the received signal in steady state with N_f number of steady state blocks and $\boldsymbol{\alpha} = [\boldsymbol{\alpha_2}, \boldsymbol{\alpha_3}, \boldsymbol{\alpha_2}, \boldsymbol{\alpha_3}, \ldots, \boldsymbol{\alpha_2}, \boldsymbol{\alpha_3}]$ where $\boldsymbol{\alpha}_2 = \mathbf{1} \oslash \mathbf{h}_2$ and $\boldsymbol{\alpha}_3 = \mathbf{1} \oslash \mathbf{h}_3$. Here, $\oslash$ denotes element-wise division. Since the original received signal does not has any correlation, we need to modify the received signal. We denote the modified steady state FBMC signal as $z[n]$ and it is given by

$$z[n] = y'[n]\alpha[n]. \tag{5}$$

To see how this modification reveals autocorrelation property, look at the idealized scenario shown in Fig. 7 showing the two blocks of output in steady state frame. If we multiply the first block by $\boldsymbol{\alpha}_2$ and second block by $\boldsymbol{\alpha}_3$, then the resultant two blocks of $\mathbf{z}$ have same samples corresponding to $\mathbf{x}_{13}$ resulting in correlation as shown in Fig. 7.

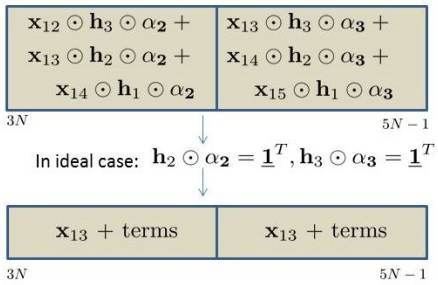

Fig. 7: Two blocks from steady state frame of PPN1 of $z[n]$. Idealized scenario which reveals correlation between samples at $\tau = N$.

In practical implementations, division by $h[n]$ is not possible as a few indices of $\mathbf{h}$ containing very small values (tending to zero) will result in implementation issues such as values going to infinity. So, we modify the definition of $\boldsymbol{\alpha}$ by introducing indicator function and a parameter δ such that

$$\alpha_k[n] = \frac{1}{h_k[n]} \cdot I_k(n, \delta), \tag{6}$$

where

$$I_k(n,\delta) = \begin{cases} 1 & h_k[n] > \delta \\ 0 & \text{otherwise,} \end{cases}$$

for $k = 2, 3$.

Now, ACF of PPN1 of $z[n]$, denoted as $R_{z1}(n, N)$, for these two blocks is given theoretically by (4). Note that the ACF of PPN2 part is derived similarly and is not included in this paper for conciseness. The ACF of $z[n]$ is sum of ACF of PPN1 and PPN2 of $z[n]$. With the proposed modification, the Nyquist nature of filter is destroyed. Hence, the autocorrelation value is non-zero at the lag N. From Fig. 8, it is evident

$$\begin{aligned}
R_{z1}(n,N) =& E\Big\{ (x_{12}[n]h_3[n]\alpha_2[n] + x_{13}[n]h_2[n]\alpha_2[n] + x_{14}[n]h_1[n]\alpha_2[n]) \\
& (x_{13}[n]h_3[n]\alpha_3[n] + x_{14}[n]h_2[n]\alpha_3[n] + x_{15}[n]h_1[n]\alpha_3[n])^* \Big\} \\
&= E\big\{x_{13}[n]h_2[n]\alpha_2[n]x_{13}^*[n]h_3[n]\alpha_3[n] + x_{14}[n]h_1[n]\alpha_2[n]x_{14}^*[n]h_2[n]\alpha_3[n]\big\} \\
&(\because E\{x_l[n]x_m[n]\} = 0 \text{ for } l \neq m) \\
&= \big(h_2[n]h_3[n]\alpha_2[n]\alpha_3[n]\big)E\big\{x_{13}[n]x_{13}^*[n]\big\} + \big(h_1[n]h_2[n]\alpha_2[n]\alpha_3[n]\big)E\big\{x_{14}[n]x_{14}^*[n]\big\} \\
&= \big(h_2[n]h_3[n]\alpha_2[n]\alpha_3[n]\big)\sigma_{x_{13}}^2 + \big(h_1[n]h_2[n]\alpha_2[n]\alpha_3[n]\big)\sigma_{x_{14}}^2 \\
&= \sigma_x^2(h_2[n]h_3[n]\alpha_2[n]\alpha_3[n] + h_1[n]h_2[n]\alpha_2[n]\alpha_3[n]) \ \ (\text{for } \sigma_{x_{13}}^2 = \sigma_{x_{14}}^2 = \sigma_x^2).
\end{aligned}$$

In ideal case, $h_2[n]\alpha_2[n] = 1,\ \ h_3[n]\alpha_3[n] = 1.$

$$\therefore R_{z1}(n,N) = \sigma_x^2(1 + h_1[n]\alpha_3[n]) \tag{4}$$

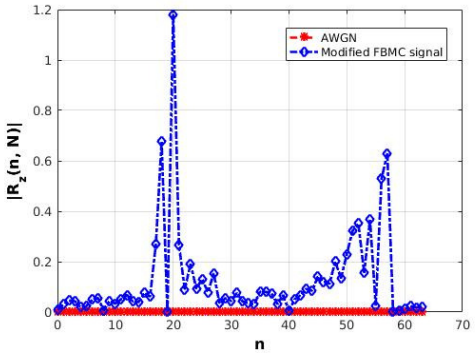

Fig. 8: Plot of $|R_z(n,N)|$. The number of Monte-Carlo realizations = 10000. The correlation value at lag of N is zero for AWGN case since noise samples are uncorrelated where as the correlation value is non-zero for modified FBMC signal because of correlated FBMC samples.

that autocorrelation function of modified FBMC signal $z[n]$ has non-zero values at lag of $\tau = N$. On the other hand, the AWGN samples, being independent, will not exhibit any autocorrelation property except at zero lag as shown in Fig. 8. Thus, this autocorrelation feature at lag of $\tau = N$ for the modified received FBMC signal can be used to detect and differentiate between FBMC signal and noise signals.

IV. Proposed Autocorrelation Detector

In this section, we propose a detection scheme to detect FBMC signal based on autocorrelation feature explored in the earlier section. We first start with presenting the system model, followed by proposed test statistic. Next, we derive the distribution of the test statistic assuming Neyman-Pearson (NP) detection criterion.

The problem of detecting the presence or absence of FBMC signal is modeled as a binary hypothesis testing problem. In our case, the binary hypothesis problem is to choose between the two hypotheses: H_0 (noise-only hypothesis) and H_1 (FBMC-signal-plus-noise hypothesis). Note that the detection is done over the modified observations. The modified received signal taking into account the AWGN noise under the two hypotheses will be given as

$$\begin{aligned} H_0: \quad u[n] &= w'[n];\ n = 0, 1, \ldots N_s - 1 \\ H_1: \quad u[n] &= z[n] + w'[n];\ n = 0, 1, \ldots N_s - 1 \end{aligned} \tag{7}$$

where $u[n]$ is the estimated signal, $w'[n] = w[n]\alpha[n]$, $w[n]$ is the AWGN noise signal, $z[n] = y'[n]\alpha[n]$ is the FBMC signal to be detected and $N_s = N_f N$ is number of samples. The proposed test statistic T for our problem is given by

$$T = \sum_{n=0}^{N-1} \frac{|\hat{R}_u(n,N)|^2}{\sigma_{rn}^2}, \tag{8}$$

where $\hat{R}_u(n,N)$ is the maximum likelihood estimate of $R_u(n,N)$ based on the observations and is given by

$$\hat{R}_u(n,N) = \frac{1}{N_f} \Re\left\{ \sum_{n_f=0}^{N_f-1} u[n+n_f N] u^*[n+n_f N+N] \right\}, \tag{9}$$

where σ_{rn}^2 is the variance of $\hat{R}_u(n,N)$ under H_0 hypothesis, N_f is total number of data blocks present in the received FBMC signal. We employ Neyman-Pearson detection criterion which maximizes the probability of detection for a given false alarm rate so that H_1 is decided if $T > \gamma$ and H_0 is decided if $T < \gamma$. Now, we need to derive the distribution of T under H_0, which in turn depends on the distribution of $\hat{R}_u(n,N)$.

A. Distribution of $\hat{R}_u(n,N)$ under H_0

Using central limit theorem for sufficiently large N in (9), we can approximate $\hat{R}_u(n,N)$ as a Gaussian random variable. The mean of $\hat{R}_u(n,N)$ under H_0 hypothesis is given by

$$\begin{aligned} &E[\hat{R}_u(n,N)|H_0] = \\ &E\left\{ \frac{1}{N_f} \sum_{n_f=0}^{N_f-1} u[n+n_f N] u^*[n+n_f N+N] \right\}. \end{aligned} \tag{10}$$

Under H_0, $u[n] = w'[n] = w[n]\alpha[n]$. So, $E[\hat{R}_u(n,N)|H_0]$ becomes

$$\begin{aligned} E\Bigg\{ \frac{1}{N_f} \sum_{n_f=0}^{N_f-1} & w[n+n_f N]\alpha[n+n_f N] \\ & w^*[n+n_f N+N]\alpha^*[n+n_f N+N] \Bigg\} = 0, \end{aligned} \tag{11}$$

since noise values are uncorrelated for $\tau = N$.

If S is a complex Gaussian random variable with variance σ^2 then $\Re\{S\}$ will also be a Gaussian random variable with variance $\frac{\sigma^2}{2}$. Variance of $\hat{R}_u(n,N)$ is given by

$$\text{Var}[\hat{R}_u(n,N)|H_0] = \frac{E[\hat{R}_u^2(n,N)|H_0] - E^2[\hat{R}_u(n,N)|H_0]}{2} \tag{12}$$

Now,

$$\begin{aligned} E[\hat{R}_u^2(n,N)|H_0] = E\Bigg\{ \Bigg(\frac{1}{N_f} \sum_{n_f=0}^{N_f-1} & w[n+n_f N]\alpha[n+n_f N] \\ & w^*[n+n_f N+N]\alpha^*[n+n_f N+N] \Bigg)^2 \Bigg\}. \end{aligned} \tag{13}$$

Substituting (11), (13) in (12), we get

$$\begin{aligned} &\text{Var}\{\hat{R}_u(n,N)\,|\,H_0\} \\ &= \sum_{n_f=0}^{N_f-1} \frac{\alpha^2[n+n_f N]\alpha^2[n+n_f N+N](\sigma_n^2)^2}{2N_f^2}. \end{aligned} \tag{14}$$

Hence, the distribution of $\hat{R}_u(n,N)$ under H_0 is given as

$$\mathcal{N}(0,\ \sigma_{rn}^2), \tag{15}$$

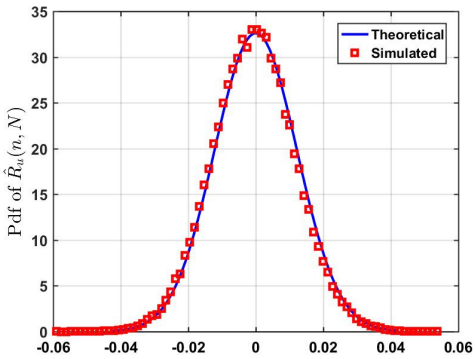

Fig. 9: The theoretical and simulated pdfs of $\hat{R}_u(n,N)$ under H_0. The number of Monte-Carlo realizations = 10000.

where

$$\sigma^2_{rn} = \sum_{n_f=0}^{N_f-1} \frac{\alpha^2[n+n_fN]\alpha^2[n+n_fN+N](\sigma^2_n)^2}{2N_f^2}. \quad (16)$$

Fig. 9 shows that the theoretical and simulated Gaussian distribution of $\hat{R}_u(n,N)$. It can be seen that both the curves match very well.

B. Distribution of T under H_0

Since the distribution of $\hat{R}_u(n,N)/\sigma_{rn}$ is a standard Gaussian random variable, the sum of squares of N such IID Gaussian random variables follow central Chi-Square distribution with N degrees of freedom.

$$\begin{aligned} P_{FA} &= Pr\{T > \gamma | H_0\} \quad (17)\\ &= Q_{\chi^2_N}(\gamma), \end{aligned}$$

where $Q_{\chi^2_N}$ is the right tail probability for a Chi-Square random variable. The threshold, γ, for the detection is obtained from probability of false alarm (P_{FA}) as (refer [14], chapter 5)

$$\gamma = Q^{-1}_{\chi^2_N}(P_{FA}). \quad (18)$$

V. Results

All the simulations are performed in MATLAB with the following parameters: $K = 3$, $N = 64$, number of blocks $= 100$, $\tau = N$. All the simulations are performed for AWGN channel. From Fig. 8, we conclude that the proposed modification to the received FBMC signal extracts the autocorrelation property which helps detecting the FBMC signal. The detection is performed assuming that noise power is known. The threshold γ of Neyman-Pearson criteria is evaluated from the distribution of T with $P_{FA} = 0.1$ under H_0.

Fig. 10 shows the probability of detection (P_D) Vs SNR [dB] curve for different δ values with $K = 3, N = 64, P_{FA} = 0.1$ for the proposed autocorrelation based detection scheme. SNR [dB] is defined as $10\log(\frac{\sigma^2_z}{\sigma^2_n})$. The results, as shown in Fig. 10, suggest that FBMC signal can be detected in presence of noise using autocorrelation

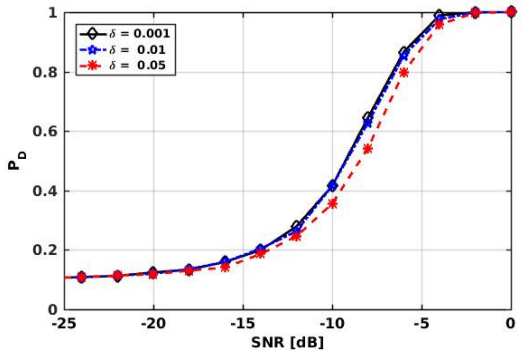

Fig. 10: P_D Vs SNR [dB] plot for FBMC signal for $P_{FA} = 0.1$ with $N = 64$ and the number of Monte-Carlo realizations = 10000.

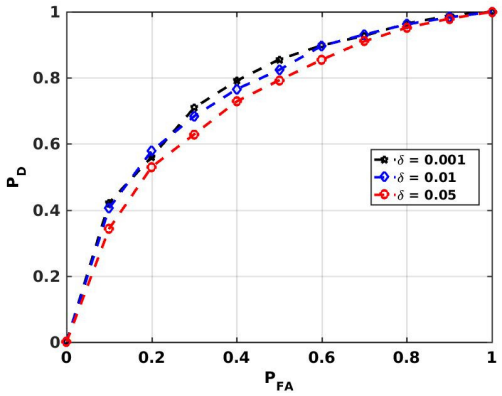

Fig. 11: Receiver operating characteristic (ROC) curves for FBMC signal for SNR = -10 dB with $N = 64$. The number of Monte-Carlo realizations = 10000.

property. The proposed detector is efficient in that the probability of detection is good even for low SNR values. Note that the threshold for the detector has been set theoretically using (18) for $P_{FA} = 0.1$. From Fig. 10, it is clear that the detector maintains the false alarm probability set of $P_{FA} = 0.1$ in simulation results under extremely low SNR values (< -30 dB), which is equivalent to H_0. In Fig. 10, there is a clear trend of decrease in the performance of the detector for values of $\delta > 0.01$. This is due to the fact that as δ value increases more number of samples of $\alpha[n]$ becomes zero, as given in (6) , and hence more number of samples of $z[n]$ that contribute to autocorrelation becomes zero. However, for low values of $\delta \leq 0.01$, the number of samples of $z[n]$ going to zero is very few. Hence, the performance of the detector is almost similar for $\delta \leq 0.01$

Receiver operating characteristic (ROC) curves for SNR$=-10$ dB for different δ values with $K = 3, N = 64$ is shown in Fig. 11. It is evident from the figure that the performance of the proposed detector is good. Unlike blind detectors like energy detector that can only sense the presence of primary

signals, the proposed detector can differentiate between FBMC signal from other primary signals. Though the overlapping factor considered in this work is $K = 3$, the findings in this paper can readily be applicable to other overlapping factors, such as $K = 4$. Although the proposed algorithm assumes AWGN channel model, this work will serve as a base for future studies on performance analysis of the algorithm for multipath fading and shadowing channels.

VI. Conclusion

In this paper, we have demonstrated that FBMC signal does not have any autocorrelation property. However, after suitably modifying the received signal, the autocorrelation property is clearly visible. This property is used to differentiate between noise-only and FBMC-plus-noise scenarios. A detector is proposed and distribution of test statistic under the noise-only scenario is derived so that the threshold for the Neyman-Pearson detector can be designed. It is demonstrated that the proposed autocorrelation detector has good performance. Further research would be carried out to analyze the performance of the detector under unknown noise variance scenario.

Acknowledgement

This work was supported by the Science and Engineering Research Board, Department of Science and Technology, India under grant no. ECR/2015/000010.

References

[1] G. Wunder, P. Jung, M. Kasparick, T. Wild, F. Schaich *et al.*, "5GNOW: non-orthogonal, asynchronous waveforms for future mobile applications," *IEEE Communications Magazine*, vol. 52, no. 2, pp. 97–105, February 2014.

[2] B. Farhang-Boroujeny, "Filter bank multicarrier modulation: A waveform candidate for 5G and beyond," *Advances in Electrical Engineering*, 2014.

[3] ——, "OFDM versus filter bank multicarrier," *IEEE signal processing magazine*, vol. 28, no. 3, pp. 92–112, 2011.

[4] PHYDAS, "Physical layer for dynamic spectrum access and cognitive radio," Online, 2010, (Accessed: Apr. 2016). [Online]. Available: http://www.ict-phydyas.org/

[5] M. Bellanger, D. Le Ruyet, D. Roviras, M. Terré, J. Nossek, L. Baltar, Q. Bai, D. Waldhauser, M. Renfors, T. Ihalainen *et al.*, "FBMC physical layer: a primer," *PHYDYAS, January*, 2010.

[6] S. Chaudhari, "Spectrum sensing for cognitive radios: Algorithms, performance and limitations," Ph.D. dissertation, Aalto University School of Electrical Engineering, Nov. 2012.

[7] B. Gao, J.-M. Park, Y. Yang, and S. Roy, "A taxonomy of coexistence mechanisms for heterogeneous cognitive radio networks operating in TV white spaces," *IEEE Wireless Communications*, vol. 19, no. 4, pp. 41–48, Aug. 2012.

[8] J.-B. Doré, R. Gerzaguet, N. Cassiau, and D. Ktenas, "Waveform contenders for 5G: Description, analysis and comparison," *Physical Communication*, 2017.

[9] R. Tandra and A. Sahai, "SNR Walls for Signal Detection," *IEEE J. of Sel. Topics in Signal Process.*, vol. 2, no. 1, pp. 4–17, 2008.

[10] H. Zhang, D. Le Ruyet, and M. Terré, "Spectral correlation of multicarrier modulated signals and its application for signal detection," *EURASIP Journal on Advances in Signal Processing*, vol. 2010, no. 1, p. 1, 2009.

[11] M. Aldababseh, "Channel estimation for FBMC/OQAM wireless system based on Kalman filter," Master's thesis, Al-Quds University, 2010.

[12] U. Madhow, *Introduction to Communication Systems*. Cambridge, 2014.

[13] M. G. Bellanger, "Specification and design of a prototype filter for filter bank based multicarrier transmission," in *IEEE International Conference on Acoustics, Speech, and Signal Processing, 2001, (ICASSP'01).*, vol. 4. IEEE, 2001, pp. 2417–2420.

[14] S. Kay, *Fundamental of Statistical Signal Processing: Volume II Detection Theory*. Prentice Hall, 1998.